

# 1

INJURY SCIENCE RESEARCH  
*Proceedings of the Twenty-Eighth International Workshop*

## **Nonlinear Viscoelastic Behavior of Brain Tissue in Oscillatory Shear Deformation**

K. K. Darvish and J. R. Crandall

### **ABSTRACT**

*Two nonlinear constitutive models were used to describe the dynamic viscoelastic behavior of brain tissue. Small disc-shaped samples of bovine brain tissue were tested in simple shear forced vibrations (0.5 to 200 Hz) with finite amplitudes (up to 20% Lagrangian shear strain). The samples response to simple, double, and triple harmonic inputs were determined to characterize the nonlinearities of up to the third-order. A quasilinear viscoelastic model was proposed to describe the spatial nonlinearity. A fully nonlinear viscoelastic model with product-form multiple hereditary integrals was proposed to describe the spatial as well as the temporal nonlinearities. The fully nonlinear model was superior at high frequencies (above 44 Hz). Under finite strains the linear complex modulus showed nonrecoverable asymptotic strain conditioning behavior. The discrepancies observed in the previous studies and the threshold of functional failure of the neural tissue were shown to be related to the strain conditioning effect.*

### **INTRODUCTION**

**T**raumatic brain injury (TBI) caused by direct impact or sudden movement of the head is one of the major causes of fatality and severe disabilities (Gennarelli, 1993). The development of particular TBI begins with mechanical deformation of the skull, intracranial blood vessels, and brain (Thibault *et al.*, 1990). In order to study the generation and propagation of mechanical stresses and strains that can cause focal and/or diffuse brain injuries, it is necessary to have an understanding of the mechanical behavior of brain tissue. Currently, the geometry of the skull and brain can be modeled with a high degree of accuracy using the available medical imaging techniques. The key element in developing a more realistic numerical (e.g., finite element) model of the head-brain complex is to improve our knowledge of the system material properties and boundary conditions. Such models are extremely useful in studying the mechanisms of TBI, in developing better predictive measures for head injury, and in improving the injury prevention techniques such as helmets, padding, and automotive restraint systems.

Brain tissue, like most other soft tissues, exhibits viscoelastic behavior. In a typical crash scenario, brain is subjected to deformation impulses with duration of only a few milliseconds (Meaney *et al.*, 1996). Therefore, dynamic test methods are more appropriate for characterizing its viscoelastic behavior (Lockett, 1972). Although the brain material behavior is nonlinear (Mendis *et al.*, 1995; Donnelly and Medige, 1997; Takhounts, 1998), previous studies on dynamic viscoelasticity of brain tissue were all based on the assumption of linearity of the constitutive relation (Fallenstein *et al.*, 1969; Galford and

McElhaney, 1969; Wang and Wineman, 1972; Shuck and Advani, 1972; Arbogast, and Margulies, 1998). The nonlinear effects in the brain constitutive relation are of particular importance for two reasons. First, a nonlinear model is more accurate for finite deformations. The existence of finite deformation in brain under representative inertial forces has been reported by Margulies (1987) by observing the response of physical models of the head. Thibault *et al.* (1990) also showed that functional failure of the neural tissue under tension occurs at finite strain levels (15% to 20%). Second, the injury pattern predicted by a nonlinear model can be potentially very different what a linear model predicts. According to the linear theory of materials with memory, the wave produced by a step-wise input is diffusive in character, broadening with time, whereas the nonlinear theory permits the existence of self-preserving waveforms. The nonlinear theory also permits the development of discontinuities in the form of shock wave or acceleration wave (Spence, 1973).

## METHODS

In this study, the nonlinear dynamic viscoelasticity of brain tissue was investigated using the forced vibration method. By using this method, compared to the other dynamic methods (i.e., the resonance method, the free vibration method, and the wave propagation method), two particular advantages were gained: 1) vibrations with finite amplitudes were generated in the material that was necessary to produce significant nonlinearity in the response, and 2) below the sample natural frequency, the inertial forces were assumed to be negligible and the stresses and strains were related only through the constitutive relation (Lockett, 1972).

### Experimental Considerations

The brain material is almost incompressible (Stalnaker, 1969) and as a result its deformation is mainly of the shear type. Since there is currently no reliable experimental method to perform vibration tests with finite amplitude on the brain tissue *in vivo*, an *in vitro* methodology was developed in which small disc-shaped samples of brain tissue were placed between two parallel plates and were subjected to oscillatory shear deformation (Figure 1). Torsional deformation was not considered because samples of brain tissue under finite angular deformation are likely to go unstable and buckle and in addition, interpretation of the experimental results will be more complicated.

*Samples Preparation.* Four bovine brains were obtained immediately after the animals (age < 1 year) were slaughtered. Bovine brains were used because of their availability. It has been shown that in stress relaxation tests, the viscoelastic behavior of bovine brain is close to that of human brain (Takhounts, 1998). During transportation and storage, the tissues were submerged in a solution of physiological saline

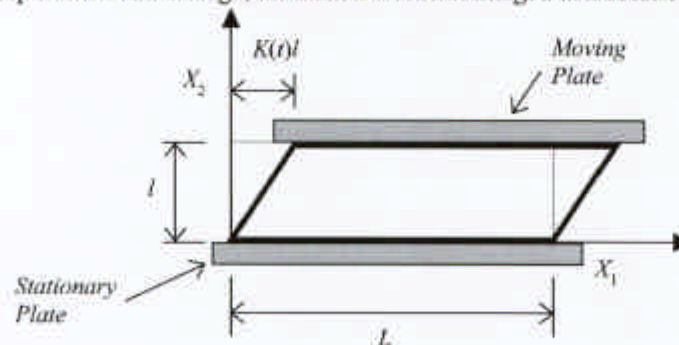


Figure 1. Shear deformation of the samples in  $X_1$  direction,  $X_2$  is along the longitudinal axis of the sample, and  $l/L \ll 1$

and bovine serum that simulated the cerebrospinal fluid. The solution temperature was kept at about 0°C. The brains were cut into thin slices (4.8 mm) within 24 hours postmortem. Two brains were sliced in the sagittal direction, one in the anterior/posterior direction, and one in the transverse direction to evaluate the effect of anisotropy (Table 1). The above directions were chosen because of the ease of extracting samples and implementing the anisotropic material properties in a finite element model of the brain. It is expected that the neural tissue is transversely isotropic with the plane of symmetry being perpendicular to the nerve fibers (Arbogast, and Margulies, 1998). With few exceptions (e.g., brain stem and corpus callosum) the directions of nerve fibers in brain are very complicated. A detailed topography of these directions is needed before a realistic anisotropic model of the brain can be developed. The total storage time of a slice in the refrigerator, before excision of the samples, was between 3 to 16 days (average = 12 days). Subsequent test results showed no correlation between the storage time and the variation in mechanical properties. Additionally, as it will be discussed later, the measured linear material properties were close to the available data in the literature with storage time less than 24 hours. Therefore, it was assumed that the postmortem material properties were preserved under the described storage method. Disc-shaped samples (15 to 20 mm diameter) were extracted from the cerebral neural tissue (corona radiata) perpendicular to the slice surface. The amount of gray matter in the samples was estimated based on its surface area compared to the white matter. Samples with 0% to a maximum of 40% gray matter were selected for testing and were assumed to be homogeneous and isotropic.

Table 1. General Specifications of the Samples.

Number	Sample ID <sup>(1)</sup>	Brain Number	Section Direction <sup>(2)</sup>	Section Number	Sample Location <sup>(3)</sup>	Material <sup>(4)</sup>	Weight (gm)	Area (mm <sup>2</sup> ) <sup>(5)</sup>	Average Density (kg/m <sup>3</sup> )
1	B1-3-2	1	1	3	posterior - left	W + <20%G	0.7	174.25	845.74
2	B1-5-2	1	1	5	posterior right	W + <10%G	1.9	397.21	1007.02
3	B1-6-1	1	1	6	Left	W + <10%G	0.9	217.11	872.70
4	B2-4-1	2	3	4	anterior left	W + <40%G	1.1	245.11	944.79
5	B3-3-1	3	2	3	center	W	2.1	479.76	921.52
6	B4-3-1	4	1	3	posterior -right	W + <5%G	1.0	230.86	911.92
7	B4-5-1	4	1	5	anterior - left	W	2.2	439.95	1052.75
8	B4-7-1	4	1	7	not recorded	W + <30%G	2.7	562.81	1009.96

<sup>(1)</sup> Sample ID's as given in Darvish (2000); <sup>(2)</sup> Direction 1: sagittal, numbered from the base of the brain. Direction 2: transverse, numbered from left. Direction 3: posterior to anterior. Each section was 4.8 mm thick. <sup>(3)</sup> Sample location is given with respect to the location of the lateral ventricles in the section; <sup>(4)</sup> W = white matter, G = gray matter. Percentages of the gray matter were estimated based on its surface area in the samples; <sup>(5)</sup> Areas were measured by approximating the samples cross-sections as ellipses. All samples were compressed to 4.75 mm thickness (1.0%) during the test.

*Test Apparatus.* Samples were attached to the stationary and moving plates with approximately 0.3 mm layer of cyanoacrylate instant adhesive (Loctite, CT, model 454 Prism) and were compressed by 1.0% between the two plates to 4.75 mm thickness to ensure secure adhesion in large deformation. The mechanical excitation of the moving plate was provided with a digitally controlled electromagnetic shaker (Vibration Test Systems, OH, model VTS 65) with 290 N maximum peak force, 19 mm stroke and DC-6500 Hz frequency response (Figure 2). The reaction shear force at the stationary plate was measured using uniaxial piezoresistive load cell (Sensotec, OH, model 31) with 2.45 N (250 gf) full scale, 27.5 mV/N sensitivity and 5.74 kHz bandwidth. The computer programs required for signal generation, data acquisition, and digital signal processing were developed in-house using LabVIEW graphical programming software (National Instruments, TX, version 5.1). Each sample was tested immediately after excision from the slice and its temperature during the test was maintained at the body temperature (37°C) by spraying warm saline solution on it.

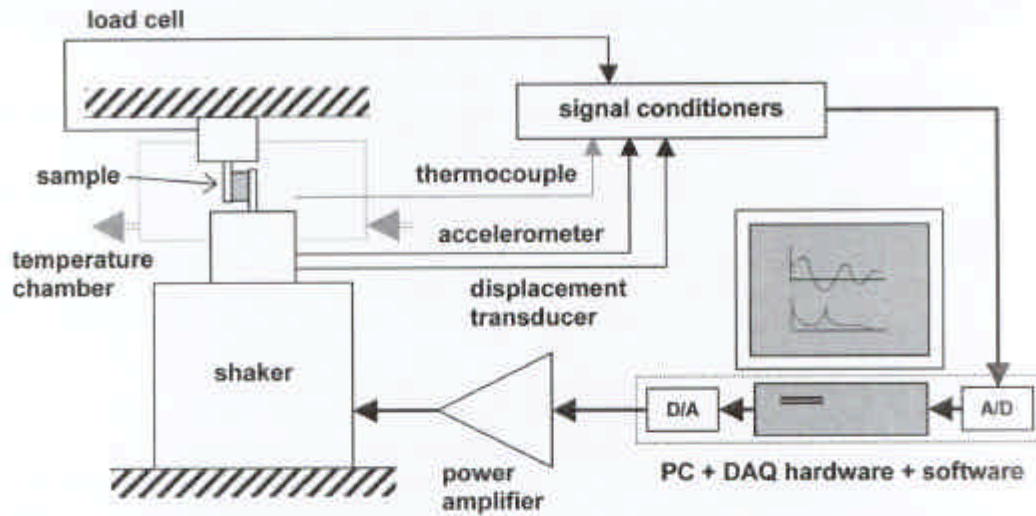


Figure 2. Schematic diagram of the experimental apparatus.

### Constitutive Models

Two nonlinear viscoelastic constitutive models were considered, namely the nonlinear viscoelastic model with *Multiple Hereditary Integrals* (MHI) and the Green-Rivlin model (Lockett, 1972) and the *Quasilinear Viscoelastic* (QLV) model with a single hereditary integral (Fung, 1993). The MHI model is nonlinear with respect to strain (spatial nonlinearity) as well as time (temporal nonlinearity) while the QLV model is nonlinear only with respect to strain. For the sake of simplicity, it was assumed that the material was moderately nonlinear of the *third-order*. This assumption was supported by the fact that functional failure of brain tissue occurs at Lagrangian shear strain levels of 10% to 15% (Thibault *et al.*, 1990; Ueno *et al.*, 1996). A constitutive model for brain tissue is practically useful at strain levels below the threshold of its functional failure.

The sample deformation was modeled as simple shear defined by:

$$x_1 = X_1 + K(t)X_2, \quad x_2 = X_2, \quad x_3 = X_3 \quad (1)$$

where  $x_i$  and  $X_i$  represent the spatial and material coordinates respectively and  $K(t)$  is the amount of shear (Figure 1). A finite element model (800 hexahedral solid elements) of a sample (20 mm diameter and 4.75 mm thickness) with isotropic material properties of Shuck and Advani (1972) was developed to evaluate the assumed deformation field and the effect of geometric nonlinearity in the sample response. The model was solved with LS-DYNA (LSTC, CA, version 950). Since the simple shear deformation is isochoric, the incompressibility condition was assumed to be satisfied regardless of the magnitude of  $K(t)$ .

*The MHI Model.* Using the MHI constitutive model the sample shear stress can be written as (Darvish, 2000):

$$\begin{aligned}
 \Sigma_{12}(t) = \Sigma_{21}(t) = & \int_0^t \psi_1(t-\tau_1) \dot{E}_{12}(\tau_1) d\tau_1 \\
 & + 4 \int_0^t \int_0^t \psi_2(t-\tau_1, t-\tau_2) \dot{E}_{12}(\tau_1) E_{12}(\tau_2) \dot{E}_{12}(\tau_2) d\tau_1 d\tau_2 \\
 & + \int_0^t \int_0^t \int_0^t \psi_3(t-\tau_1, t-\tau_2, t-\tau_3) \dot{E}_{12}(\tau_1) \dot{E}_{12}(\tau_2) \dot{E}_{12}(\tau_3) d\tau_1 d\tau_2 d\tau_3
 \end{aligned} \quad (2)$$

in which  $\Sigma_{12}(t)$  is the shear component of the “transformed back” or “pulled back” Cauchy stress tensor to the frame that is rotated with the rotation component of the deformation gradient at time  $t$ :

$$\Sigma_{12} = \Sigma_{21} = \sigma_{12} + \frac{1}{2} K \Delta\sigma_n - \frac{1}{2} K^2 \sigma_{12} - \frac{1}{8} K^3 \Delta\sigma_n \quad (3)$$

where  $\Delta\sigma_n = \sigma_{11} - \sigma_{22}$  is the “normal stress effect” due to large rotations, and  $E_{12} = E_{21} = \frac{1}{2} K$  is the Lagrangian shear strain. The second integral in equation (2) is due to the normal strain  $E_{22} = \frac{1}{2} K^2$  present in finite shear deformation.  $\psi_1$ ,  $\psi_2$ , and  $\psi_3$  are the first-, second-, and third-order material relaxation kernel functions respectively. These functions, for all real materials, are symmetric with respect to multiple time arguments  $t - \tau_k$  ( $k = 1, 2, 3$ ), monotonically decreasing for  $t - \tau_k \geq 0$ , and identically zero for  $t - \tau_k < 0$ . It should be noted that in derivation of equation (1), to account for temporal nonlinearity, all the possible “cross-effects” or “interactions” are considered to be present in the higher-order kernel functions. In addition, it is assumed that the material has no plastic deformation and it is “non-aging”, i.e., its material properties do not vary with time. The MHI model has had very limited experimental applications because of the large number of experimental data that is needed for characterizing its material properties and *ad hoc* nonlinear models were used instead (Findley *et al.*, 1976). With the advancements in digital data acquisition and signal processing, characterization of the MHI model has become now feasible. The major advantages of the MHI model with respect to *ad hoc* nonlinear models are 1) it is general purpose, i.e., it can be used for any loading condition and 2) it can describe all the possible nonlinearities in the response of materials with memory, namely the spatial and temporal nonlinearities.

*The QLV Model.* To assure a nonlinear response in shear, the elastic response of the QLV model was assumed to be governed by a second-order Rivlin strain energy density function:

$$W = C_{10}(I_1 - 3) + C_{01}(I_2 - 3) + C_{11}(I_1 - 3)(I_2 - 3) \quad (4)$$

where  $C_{10}$ ,  $C_{01}$ , and  $C_{11}$  (all positive) are the material constants, and  $I_1$  and  $I_2$  are the first and second invariants of the left Cauchy-Green strain tensor. The sample shear stress can be written as (Darvish, 2000):

$$\sigma_{12} = \sigma_{21} = 2\mu_0 \int_0^t G(t-\tau) [1 + 12\gamma e_{12}^2(\tau)] \dot{e}_{12}(\tau) d\tau \quad (5)$$

in which  $e_{12} = e_{21} = \frac{1}{2} K$  is the Eulerian shear strain, and  $\mu_0 = 2(C_{10} + C_{01})$  and  $\gamma = 2C_{11}/(C_{10} + C_{01})$  are the linear elastic shear modulus and the nonlinearity coefficient respectively.  $G(t)$  is the reduced relaxation function that describes the time dependency of the response ( $0 < G(t) \leq 1$  with  $G(0) = 1$ ). The important additional assumption in equation (5), compared to equation (2), is that the “cross-effects” are neglected. Therefore the QLV model is linear with respect to time and nonlinear only with respect to

strain. Since it has a single hereditary integral, the QLV model, compared to the MHI model, requires less experimental data for material characterization.

### Dynamic Material Characterization

The third-order nonlinear material properties were characterized by applying simple, double, and triple harmonic inputs. The MHI model (equation 2) is considered subject to superposition of  $n$  harmonic shear strain inputs that can be written as:

$$E_{12}(t) = \sum_{k=1}^n A_k \sin(\omega_k t) \quad (6)$$

in which  $A_k$  and  $\omega_k$  represent the input amplitudes and frequencies respectively. Roman numeric (*I, II, III*, etc) is used for the frequency index. For a simple harmonic input ( $n = I$ ), the stress response can be written as:

$$\begin{aligned} \Sigma_{12}(t) = R_I^1 = & [A_I E_1(\omega_I) + \frac{3}{4} A_I^3 E_3(\omega_I, \omega_I, -\omega_I)] \sin(\omega_I t) \\ & - \frac{1}{4} A_I^3 E_3(\omega_I, \omega_I, \omega_I) \sin(3\omega_I t) \end{aligned} \quad (7)$$

in which  $E_1(\cdot)$  and  $E_3(\dots)$  represent the linear and the third-order complex moduli defined by:

$$E_1(\omega_1) = i\omega_1 \bar{\psi}_1(\omega_1) \quad (8)$$

$$\begin{aligned} E_3(\omega_1, \omega_2, \omega_3) = & -4\omega_1 \omega_2 \omega_3 \bar{\psi}_2(\omega_1, \omega_2 + \omega_3) \\ & - i\omega_1 \omega_2 \omega_3 \bar{\psi}_3(\omega_1, \omega_2, \omega_3) \end{aligned} \quad (9)$$

The bars over the relaxation functions represent their generalized Fourier transforms defined as:

$$\bar{\psi}_n(\omega_1, \dots, \omega_n) = \int_{-\infty}^{\infty} \dots \int_{-\infty}^{\infty} \psi_n(t_1, \dots, t_n) \exp(-i\omega_1 t_1 - \dots - i\omega_n t_n) dt_1 \dots dt_n \quad (10)$$

For double harmonic inputs ( $n = II$ ), the stress response can be written as:

$$\Sigma_{12}(t) = \sum_{k=1}^{II} R_k^1 + R_{I,II}^2 \quad (11)$$

where

$$\begin{aligned} R_{I,II}^2 = & \frac{3}{2} A_I A_{II} [A_{II} E_3(\omega_I, \omega_{II}, -\omega_{II}) \sin(\omega_I t) + A_I E_3(\omega_I, -\omega_I, \omega_{II}) \sin(\omega_{II} t)] \\ & - A_I A_{II} \sum_{k=0}^1 \left[ \frac{3}{4} A_I (-1)^k E_3[\omega_I, \omega_I, (-1)^k \omega_{II}] \sin \left\{ [2\omega_I + (-1)^k \omega_{II}] t \right\} \right. \\ & \left. + \frac{3}{4} A_{II} E_3[\omega_I, (-1)^k \omega_{II}, (-1)^k \omega_{II}] \sin \left\{ [\omega_I + (-1)^k 2\omega_{II}] t \right\} \right] \end{aligned} \quad (12)$$

For triple harmonic inputs ( $n = III$ ), the stress response can be written as:

$$\Sigma_{12}(t) = \sum_{k=1}^M R_k^1 + R_{I,II}^2 + R_{II,II}^2 + R_{I,III}^2 + R_{I,II,III}^3 \quad (13)$$

where

$$R_{I,II,III}^3 = -\frac{1}{2} A_I A_{II} A_{III} \sum_{k=0}^1 \sum_{m=0}^1 (-1)^k (-1)^m E_3[\omega_I, (-1)^k \omega_{II}, (-1)^m \omega_{III}] \sin\{[\omega_I + (-1)^k \omega_{II} + (-1)^m \omega_{III}]t\} \quad (14)$$

*Distortions in the Stress Response.* It is evident from equations (7), (12), and (14) that the stress response in the MHI model contains *intermodulation distortions* or frequency components that are combinations of the fundamental frequencies  $\omega_I$ ,  $\omega_{II}$ , and  $\omega_{III}$  and their integer harmonics (*harmonic distortions*). The frequency components of the stress response were determined from windowed Fast Fourier Transform (FFT) of the measured force and displacement signals (15 kHz sampling rate, 32 KB frame size, Exact Blackman window) (National Instruments, 1998). By changing the input frequencies independently, the linear and the third-order complex moduli were determined. Due to the symmetry of the relaxation functions with respect to their time arguments, the complex moduli are also symmetric with respect to their frequency arguments. Therefore the frequencies were selected as  $\omega_I \geq \omega_{II} \geq \omega_{III}$  during the experiment. It was practically more convenient to perform the tests in three stages: In the first stage, a single harmonic input was applied and the moduli corresponding to the harmonic distortions were determined using equation (7). In the second and the third stages, superpositions of two and three harmonic inputs were applied respectively and the moduli corresponding to the intermodulation distortions were determined using equations (11) to (14). To simplify the calculations, the frequencies were chosen such that their integer and noninteger harmonics did not overlap.

Two distortion measures were used to evaluate the nonlinearity of the response: 1) The third harmonic distortion ( $HD_3$ ) that is the relative distortion of the first 3 harmonics with respect to the fundamental frequency, and 2) The total harmonic distortion plus noise ( $TD$ ) (National Instruments, 1998).  $HD_3$  shows how much the response deviates from the linear response and  $TD$  shows that the deviation from linearity is random (e.g., due to noise) or it is because of nonlinearity in the system. When  $HD_3 = TD$  all the distortion is caused by up to the 3<sup>rd</sup>-order nonlinearity of the system. The effect of the broad distortion caused by the natural frequencies of the sample on the distortions caused by forced vibration was evaluated by directly examining the output spectrums. Although the shaker system was designed to be linear, it was inevitably slightly nonlinear (due to friction, the magnetic field, and the amplifier) especially at low frequency-large amplitude applications. The distortions of the sample were approximated by subtracting the distortions of the response (force signal) from the corresponding values of the input (displacement signal). This approximation becomes invalid when the input distortions are close to the output distortions and may lead to negative distortion measures for the material.

*The Linear Complex Modulus.* Two methods were used to determine the linear complex modulus: 1) applying simple harmonic inputs with maximum 10% root mean squared (rms) Lagrangian shear strain and sweeping the input frequencies from low to high, and 2) applying white noise input with 4.6% to 7.6% rms strain (2 kHz bandwidth, 8192 samples) and calculating the transfer function between the FFT of shear stress and the FFT of shear strain. In the second method, only a single measurement was required to determine the sample complex shear modulus, which in turn, significantly reduced the test time. However, this method is valid only for linear systems. The linearity of the response at low strain levels was verified by the coherence function (National Instruments, 1998).

The linear complex moduli were modeled using a discrete spectrum approximation:

$$E_1(\omega) = \sum_{k=0}^3 \frac{iC_k \omega}{i\omega + \beta_k} \quad (15)$$

in which  $C_k$  and  $\beta_k$  are the relaxation amplitudes and the decay rates of the associated relaxation function respectively. The first constant term was determined based on the material response at 1 Hz. The second and the third decay rates were arbitrarily chosen at  $10 \text{ s}^{-1}$  and  $100 \text{ s}^{-1}$  to perform slight local adjustments to the model. The fourth decay rate and the relaxation amplitudes were determined using an iterative scheme to optimize the mean squared error (*MSE*) and the coefficient of determination ( $R^2$ ).

The aging or time translation effect of the linear complex shear modulus of brain tissue with respect to shear strain was investigated. This phenomenon was called *strain conditioning*. Understanding the strain conditioning of brain tissue is of crucial importance for development of constitutive models that are valid for large strains and particularly repetitive loading. The variations in the magnitude and the phase of the linear complex modulus with respect to strain were determined at 5 Hz. The root-mean-squared (RMS) of Lagrangian shear strain was first increased from 3% to 21% (loading). Afterwards, the strain was decreased back to 3% (unloading). The steady-state linear complex modulus was measured at several strain levels during loading and unloading.

*The Nonlinear Complex Moduli.* In order to reduce the number of parameters of the MHI model, a product-form (PF) model (Nakada, 1960) was explored in which the  $n$ th order complex modulus can be written as:

$$E_n(\omega_1, \dots, \omega_n) = \alpha_n^p E_1(\omega_1) \dots E_1(\omega_n) \quad (16)$$

where  $\alpha_n^p$  is defined as the *coefficient of product-form nonlinearity* of the  $n$ th order. For a material with product-form nonlinearity these coefficients should be real constants (independent of the input frequencies and amplitudes). In the QLV model, it can be shown that the higher order complex moduli are linearly related to the linear complex modulus (Darvish, 2000), which can be written as:

$$E_n(\omega_1, \dots, \omega_n) = \alpha_n^q E_1(\omega_1 + \dots + \omega_n) \quad (17)$$

where  $\alpha_n^q$  is defined as the *coefficient of quasilinearity* of the  $n$ th order. For a QLV material all  $\alpha_n^q$  should be real constants. Using equation (17), the nonlinearity coefficient of the QLV model (equation 5) can be written as  $\gamma = \gamma_i \alpha_i^q$ . The third-order complex moduli were represented in two-dimensional plots by mapping the three-dimensional space of the input frequencies to a one-dimensional space of *frequency combination index (FCI)* given in the appendix (Table A-1). The third-order nonlinearity coefficients  $\alpha_1^q$  and  $\alpha_2^q$  were determined by an iterative solution technique. Three measures were used for evaluating the goodness of fit for the magnitude and the phase: 1) the average relative error (*ARE*), 2) the mean squared error (*MSE*), and 3) the coefficient of determination ( $R^2$ ). The relative error was defined as the difference between the analytical and experimental values divided by the absolute value of the experimental value.

## RESULTS

*Basic Assumptions.* In the ideal simple shear deformation the stresses and strains are expected to be constant throughout. The finite element model of samples showed that the coefficients of variation of shear strain and shear stress for 10% Lagrangian shear strain were 2.3% and 15.6% respectively. The model showed an overall geometric nonlinear effect (equation 3) of 0.42%, 0.33%, and 0.18% on the average shear stress at 10%, 20%, and 30% Lagrangian shear strain respectively. This effect was considered to be negligible and it was assumed that  $\Sigma_{12} \approx \sigma_{12}$ .

*The Nonlinear Response.* The Lissajous curves of shear stress versus Lagrangian shear strain for simple harmonic inputs showed strong nonlinearity in the viscoelastic response of the samples even at shear strains as low as 1% (Figure 3). Comparison between the computed  $HD_3$  and  $TD$  showed that the observed nonlinearity was mainly of the third-order (Figures 4 and 5). The broadband hump in the output spectra that was due to the sample natural frequencies near 440 Hz gave rise to the measured total harmonic distortions of sub-harmonics between 27 Hz and 87 Hz.

*The Linear Complex Moduli.* The magnitude of linear complex moduli showed approximately one order of magnitude rise between 10 Hz and 100 Hz (Figure 6) that was in agreement with the assumption of discrete spectrum approximation given in equation (15). A resonance of the sample holders occurred at about 60 Hz that caused a ripple in the magnitude of the complex moduli close to that frequency and disturbed the phase data above 30 Hz. Only the phase data at low frequencies (below 30 Hz for simple harmonic inputs and below 10 Hz for white noise input) were used in determination of the samples material properties. The material parameters derived for the linear complex moduli using simple harmonic input and white noise input are given in Tables 2 and 3 respectively. The results showed different anisotropic behavior at low and high frequencies (Figure 7). At 1 Hz, corresponding to the coefficient  $C_{10}$ , the moduli in the anterior/posterior and the transverse directions were about 35% lower than the modulus in the sagittal direction. At about 100 Hz, corresponding to the coefficient  $C_{30}$ , the modulus in the anterior/posterior direction was about 15% higher than the moduli in the sagittal and the transverse directions.

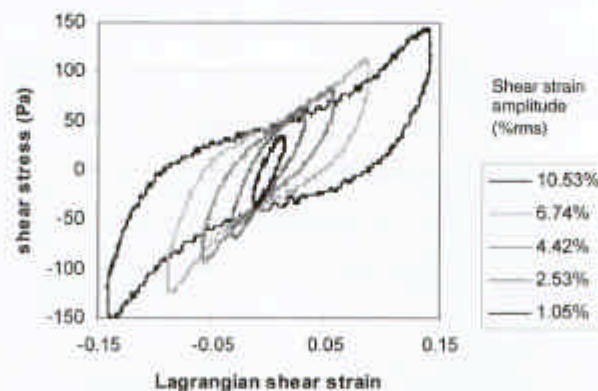


Figure 3. Lissajous curves of sample 7 at 5 Hz.

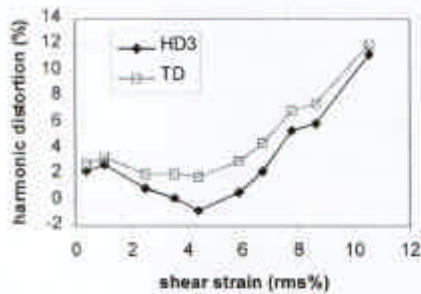


Figure 4. Harmonic distortions of sample 7 at 5 Hz.

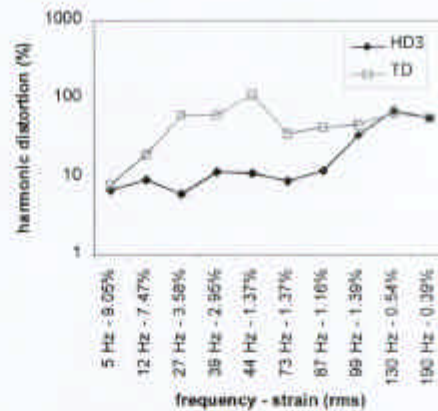


Figure 5. Harmonic distortions of sample 2.

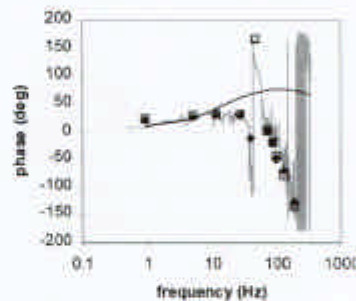
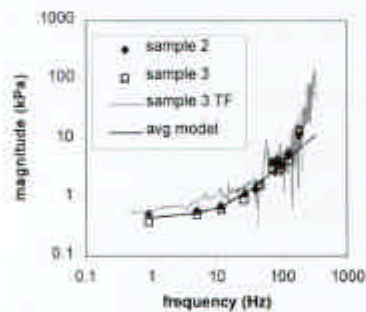


Figure 6. The linear complex moduli of samples 2 and 3 (white noise strain = 7.58% rms).

The variations in the magnitude and the phase of the linear complex shear modulus with respect to strain at 5 Hz is shown in Figure 8. The results showed strain conditioning in the form of decrease in the magnitude of the linear complex shear modulus and increase in its phase, both to asymptotic values. The loading paths of samples 2 to 5 (strain and frequency) and the magnitude of their linear complex shear moduli are plotted in the three-dimensional space of strain-frequency-modulus in Figure 9. Samples 2 and 3 were strain conditioned at 1 Hz and the magnitude of their complex moduli at 5 Hz, were slightly lower than the moduli of samples 4 and 5 (at the same strain level) that were strain conditioned at 5 Hz. This shows that strain conditioning was independent of the loading path in the strain-frequency plane.

*The Nonlinear Material Properties.* The magnitudes and phases of the experimental, the PF-MHI, and the QLV third-order complex moduli are shown in Figures 10 and 11. The calculated third-order nonlinearity coefficients ( $\alpha_3^p$  and  $\alpha_3^q$ ) are given in Table 4. For sample 6 and for the average third-order coefficients, the linear complex modulus was assumed to be the average model given in Table 2. The average Lagrangian shear strain for double and triple harmonic inputs was 12% rms with 3% standard

Table 2. Material Constants of the Linear Complex Moduli Determined from the Simple Harmonic Input Test Results.

Sample	$C_0$ (kPa)	$C_1$ (kPa)	$\beta_1$ (1/s)	$C_2$ (kPa)	$\beta_2$ (1/s)	$C_3$ (kPa)	$\beta_3$ (1/s)	Goodness of Fit in Magnitudes (< 100 Hz)		Goodness of Fit in Magnitudes (< 40 Hz)		Goodness of Fit in Phases (< 30 Hz)	
								MSE (kPa <sup>2</sup> )	R <sup>2</sup>	MSE (kPa <sup>2</sup> )	R <sup>2</sup>	MSE (deg <sup>2</sup> )	R <sup>2</sup>
2	0.48	0.07	10	0.01	100	33.0	5500	0.319	0.924	0.008	0.992	5.535	0.757
3	0.35	0.10	10	0.01	100	30.0	5500	0.082	0.936	0.008	0.987	5.374	0.819
Average	0.42	0.09	10	0.01	100	31.5	5500	0.277	0.890	0.010	0.943	5.334	0.848

Table 3. Material Constants of the Linear Complex Moduli Determined from the White Noise Input Test Results.

Sample	White Noise Strain (rms%)	$C_0$ (kPa)	$C_1$ (kPa)	$\beta_1$ (1/s)	$C_2$ (kPa)	$\beta_2$ (1/s)	$C_3$ (kPa)	$\beta_3$ (1/s)	Goodness of Fit in Magnitudes (< 100 Hz)		Goodness of Fit in Magnitudes (< 40 Hz)		Goodness of Fit in Phases (< 10 Hz)	
									MSE (kPa <sup>2</sup> )	R <sup>2</sup>	MSE (kPa <sup>2</sup> )	R <sup>2</sup>	MSE (deg <sup>2</sup> )	R <sup>2</sup>
1	4.63	0.58	0.17	10	0.05	100	31.0	5500	0.276	0.766	0.080	0.719	1.452	
4	5.68	0.37	0.20	10	0.05	100	37.0	5500	0.184	0.916	0.026	0.855	0.983	
5	7.37	0.35	0.20	10	0.05	100	33.0	5500	0.082	0.954	0.032	0.758	1.313	
8	4.84	0.80	0.30	10	0.20	100	35.0	4000	0.272	0.933	0.046	0.820	0.397	

deviation. The magnitude of the PF-MHI third-order modulus, at identical frequency arguments above 44 Hz, was significantly larger than the QLV model. However, at nonidentical frequency arguments, the magnitudes of the two models were close (Figure 12).

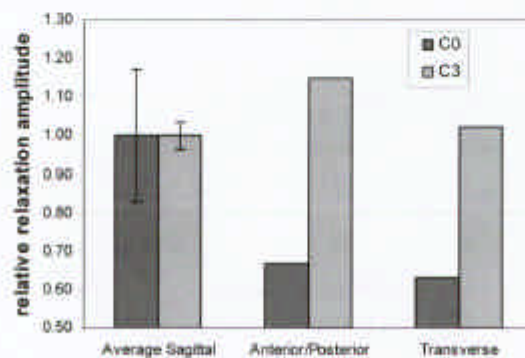


Figure 7. The relative relaxation amplitudes  $C_0$  and  $C_3$  with respect to the average sagittal values.

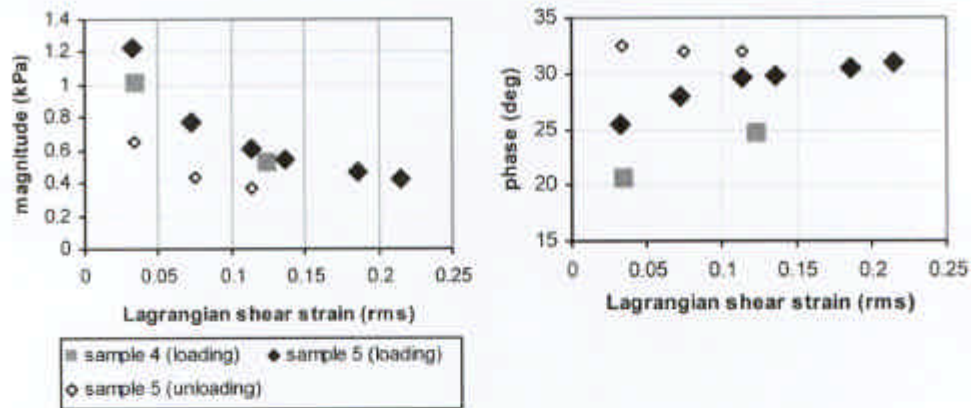


Figure 8. Strain conditioning of the linear complex moduli of samples 4 and 5 at 5 Hz.

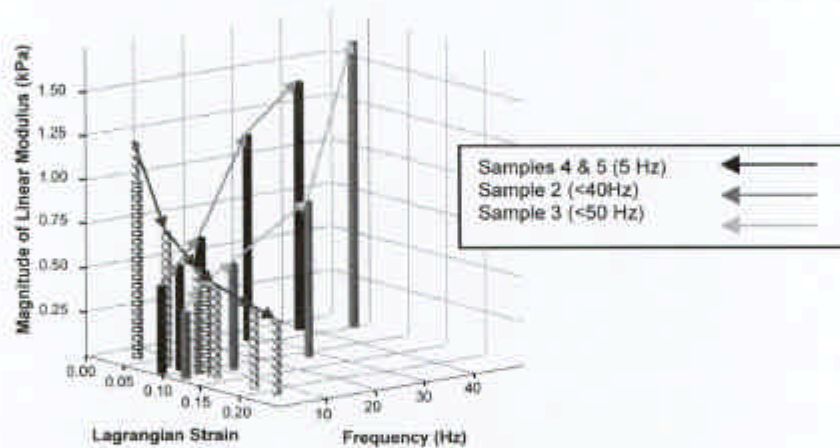


Figure 9. Magnitudes of the linear complex moduli of samples 2 to 5 with respect to strain and frequency (experiments were performed in the direction of arrows).

Based on the average linear complex modulus given in Table 2 and  $\alpha_3^q = 10.5$  (Table 4), the elastic material constants of the average QLV model were calculated as  $\mu_0 = 16.01$  kPa and  $\gamma = 2.62$ . The Rivlin material constants, assuming  $C_{10} = 0.9C_{01}$  (Mendis *et al.*, 1995), were derived as  $C_{10} = 3.79$  kPa,  $C_{01} = 4.21$  kPa, and  $C_{11} = 10.51$  kPa. The normalized elastic shear response (with respect to the elastic shear modulus  $\mu_0$ ) is shown in Figure 13.

## DISCUSSION

*Strain Hardening of the QLV Elastic Response.* The instantaneous elastic response of the QLV model showed hardening for Lagrangian shear strains above 10%. This behavior was in contradiction with the QLV models proposed by other investigators for brain tissue (Figure 13). The model of Mendis *et al.*

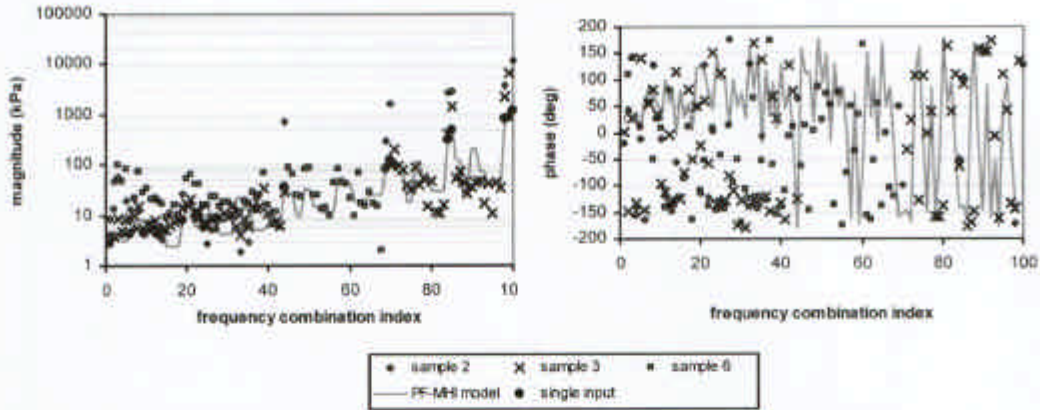


Figure 10. The experimental and the PF-MHI third-order complex moduli.

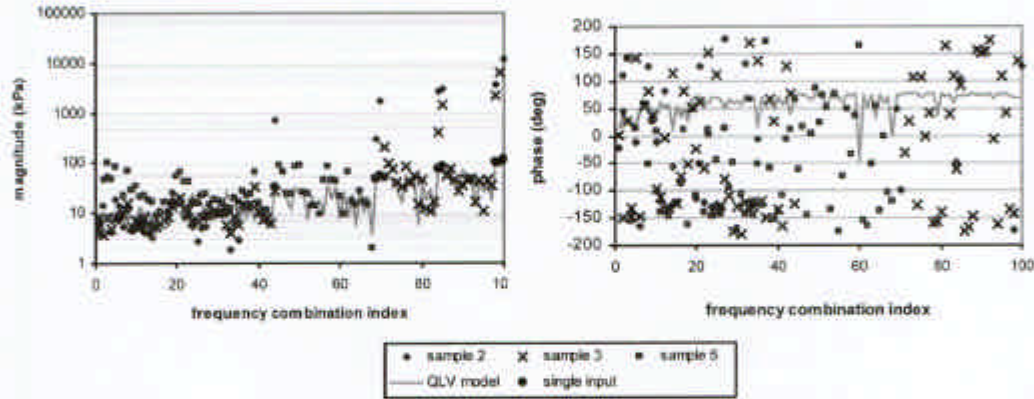


Figure 11. The experimental and the QLV third-order complex moduli.

Table 4. Material Constants of the Third-Order Complex Moduli.

Sample	Model	Third-Order Coefficient $\alpha_3^q$ or $\alpha_3^r$	ARE (%)		MSE		$R^2$	
			Mag.	Phase	Mag. ( $\text{kPa}^2$ )	Phase ( $\text{deg}^2$ )	Mag.	Phase
2	QLV	8.5	0.2	136.1	10,595,819	17,090	0.697	0.000
	PF-MHI	15.2	0.1	52.5	9,131,588	27,082	0.884	0.030
3	QLV	9.3	-0.3	207.7	852,882	20,082	0.369	0.000
	PF-MHI	19.7	-0.2	50.8	497,005	27,913	0.813	0.016
6	QLV	15.6	0.1	239.8	685	21,278	0.088	0.052
	PF-MHI	27.6	-0.3	196.9	819	29,523	0.079	0.109
Average	QLV	10.5	9.0	208.0	1,233,631	19,964	0.446	0.009
	PF-MHI	21.2	3.1	110.8	981,765	27,881	0.849	0.038

(1995), derived from uniaxial compressive stress relaxation test results, predicts a linear behavior in shear. The model of Prange *et al.* (1998), derived from shear stress relaxation tests, predicts a low rate softening behavior. The rise time in the experiments conducted by Prange *et al.* (1998) was 60 ms. The difference between the short-term elastic response, determined from the vibration test results, and the long-term elastic response, determined from the stress relaxation test results, indicates that the rate of

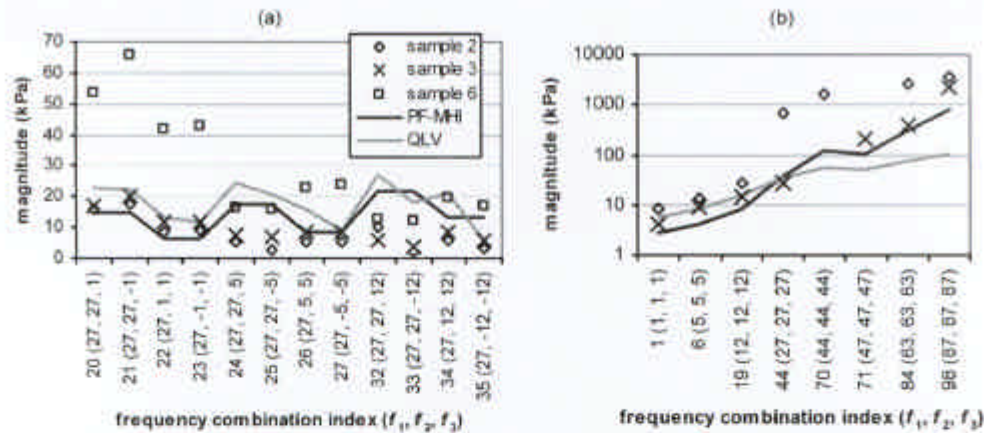


Figure 12. Selected portions of the experimental, PF-MHI, and QLV complex moduli at a) nonidentical frequency arguments and b) identical frequency arguments.

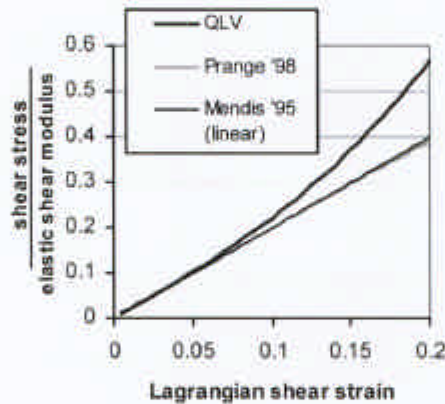


Figure 13. The normalized instantaneous elastic shear response of the proposed QLV model compared to the results of other investigators.

relaxation increases with strain. Therefore, the tissue exhibits temporal nonlinearity that is more significant in the short-term response and becomes almost negligible in the long-term response.

*The PF-MHI Model Versus the QLV Model.* Overall, the third-order PF-MHI model, compared to the QLV model, was a better predictor of the experimental results. For the magnitude of the third-order complex modulus with identical frequency arguments, at higher frequencies (above 44 Hz) the PF-MHI model was significantly superior whereas at lower frequencies the QLV model was slightly better (Figure 12a). For nonidentical frequency arguments, the two models described the experimental magnitude data almost equally (Figure 12b). Both models at low frequencies ( $FCI < 24$ ) described the lower bound of the magnitudes. Although the PF-MHI model phase data showed more variations than the QLV model, both models did not satisfactorily describe the scattered experimental phase data.

*The Linear Complex Modulus and Strain Conditioning.* It is a well-known fact that in order to establish a unique constitutive relation, biological soft tissues should be preconditioned (Fung, 1993). In this study, material characterization was based on the steady state responses and hence the samples were effectively preconditioned. Nevertheless, the results of this study showed that another form of conditioning existed

that was due to strain and was called strain conditioning. Strain conditioning was manifested as a decrease in the magnitude and an increase in the phase of the linear complex modulus to asymptotic values (Figure 8). Before the linear complex modulus became asymptotic, strain conditioning was partially recoverable and after that it was almost fully nonrecoverable. In this study, only short-term recovery, within few minutes after the initial loading, was studied. Whether long-term recovery from strain conditioning exists, especially *in vivo*, would require more investigation.

At 5 Hz input frequency, the threshold of asymptotic strain conditioning was 15% Lagrangian shear strain. This threshold appeared to decrease at higher frequencies. Below 50 Hz, the magnitudes of the linear complex moduli obtained using simple harmonic inputs were lower than the ones obtained using white noise input and their phases were higher (Figure 6). This difference can be explained based on the strain conditioning effect with regard to the fact that the low frequency rms strain amplitude of harmonic inputs (10%) was larger than the white noise rms strain amplitude (7.58% rms). However, the two moduli at frequencies above 50 Hz became indistinguishable, which indicated that both had been strain conditioned asymptotically.

The strain conditioning effect can be used to explain part of the variability that is observed in the material properties of brain tissue reported by other investigators. Generally, in previous studies, when larger strains were applied at low frequencies, lower magnitudes and higher phases were measured for the linear complex modulus. As the input frequency was gradually increased, less variability can be observed in the reported material properties (Figures 14 to 16).

The results of Arbogast and Margulies (1998) were obtained by performing oscillatory shear deformation on samples from porcine brain stem. Their results, compared to the results of this study, show a lower rise in the magnitude of the complex shear modulus and no significant viscoelastic transition below 200 Hz (Figure 14 and 15). In the present study, the discrete spectrum approximation that was selected to model the rapid rises in the magnitudes of the complex shear moduli, suggested a significant viscoelastic transition at about 150 Hz. Due to inertial effects, this transition could not be verified with the experimental phase data. Although Arbogast and Margulies (1998) applied low strain levels (2.5%, 5%, and 7.5% engineering shear strains), their results show reduction in the magnitude of the complex shear

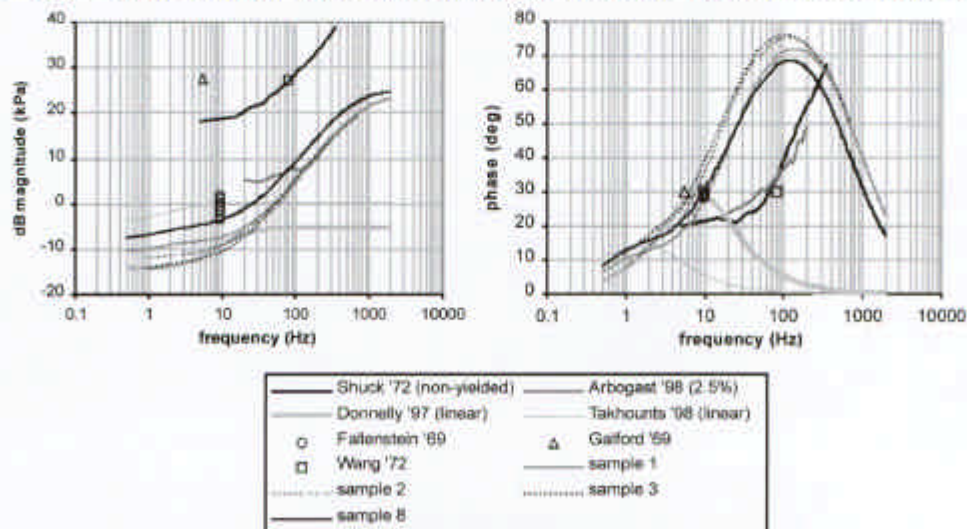


Figure 14. The linear complex shear moduli derived in this study compared to the results of other investigators.

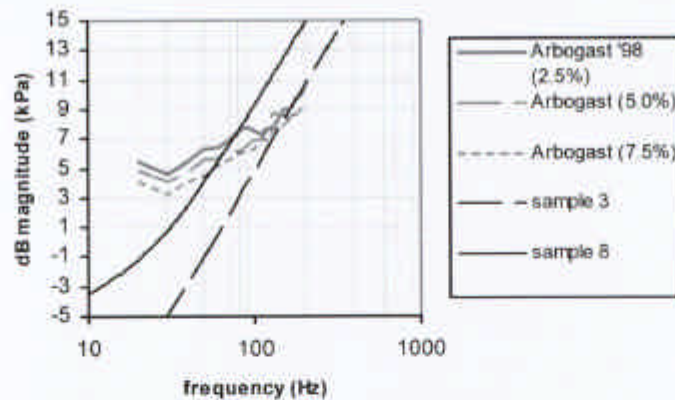


Figure 15. The magnitude of the linear complex shear moduli derived in this study compared to the results of Arbogast and Margulies (1998).

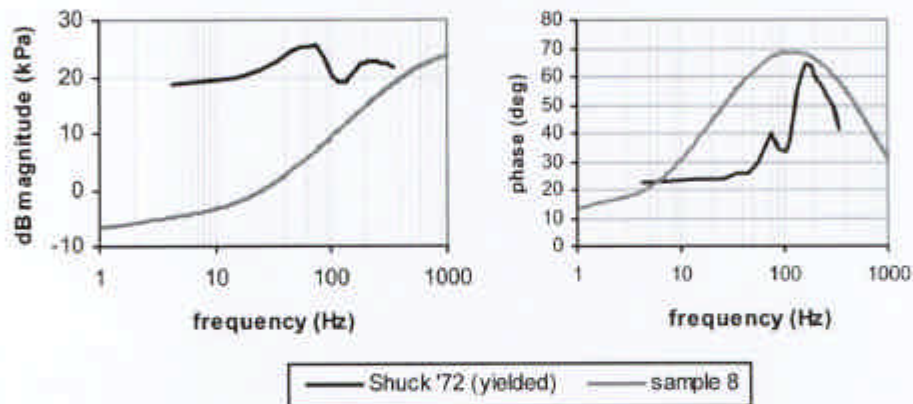


Figure 16. The linear complex shear modulus derived in this study compared to the "yielded" modulus of Shuck and Advani (1972).

modulus with strain that is due to strain conditioning (Figure 15). In addition, at frequencies above 100 Hz, all their results converge to the results of this study that can be attributed to asymptotic strain conditioning. results is high because it was approximated by

Shuck and Advani (1972) performed oscillatory torsion tests with small strains (below 3.5% engineering shear strain) on human brain tissue. In the swept sine test results (starting at low frequencies), they observed a *yielding* behavior (Figure 16). In order to avoid yielding, they applied the high frequency inputs individually, and derived relatively high magnitudes for the complex shear modulus (Figure 14). It should be noted that both magnitude and phase of their yielded results, after about 80 Hz, approaches the results of the present study which suggests that what they observed as yielding was in fact asymptotic strain conditioning.

The results of Wang and Weinman (1972) were based on *in vivo* forced vibration tests on Rhesus monkey. Their results agree very well with the "non-yielded" results of Shuck and Advani (1972). They applied only a single input frequency (80 Hz) and as result no strain conditioning was occurred. Galford and McElhaney (1969) performed free vibration tests on human brain samples in compression. The magnitude of the shear modulus corresponding to their results is high because it was approximated by

assuming a constant Poisson's ratio of 0.5. The results of Fallenstein *et al.* (1969) were obtained by studying the resonance of human brain samples in simple shear. Their results are very close to the results of the present study and show strain conditioning as they increased the engineering strain level from 7% to 24%. Takhounts (1998) conducted stress relaxation tests on human and bovine brain samples in simple shear. His proposed linear relaxation function was valid for engineering shear strains below 10%. Donnelly and Medige (1997) performed constant high strain rate tests on human brain samples with up to 100% engineering shear strain and  $180 \text{ s}^{-1}$  strain rate. The linear relaxation functions of the two latter studies that were modeled by Prony series were transformed into the frequency domain using equation (15). Since in both test methods the short-term effects could not be measured, the two models show "false saturation" at 10 Hz and 20 Hz respectively. Below the saturation frequency, their results are in agreement with the low frequency results of this study. Donnelly and Medige (1997) applied the largest strain levels and hence their results show the highest level of strain conditioning.

One possible hypothesis may be that strain conditioning is due to mechanical failure of the weaker bonds in the glia. Glial cells, that are twice as numerous as neurons, provide the structural stability of the neural tissue and form a complicated three-dimensional network. While the glial cells become fully stretched, the complex moduli reach their asymptotic values. As a result, the neural fibers become load bearing and therefore the risk of their functional failure increases. The functional failure of neural tissue at low loading rates is believed to occur in the range of 10% to 15% Lagrangian shear strain (Thibault *et al.*, 1990) which is in close agreement with the threshold of asymptotic strain conditioning (15%) found in this study at 5 Hz. Strain conditioning predicts that repetitive loading would make the brain tissue structurally weaker and therefore more susceptible to injury. More mechanical test data as well as pre- and post-test histological data of the samples are needed for better understanding of the mechanism of strain conditioning.

*Anisotropy of the Linear Complex Modulus.* Shuck and Advani (1972), using the same global axes as in this study, in the frequency range of 2 Hz to 10 Hz, observed about -30% anisotropy in the anterior/posterior and transverse directions compared to the sagittal direction. Their result is in close agreement with the results of this study at 1 Hz. However, the results of this study at higher frequencies showed that anisotropy was frequency dependent. One possible reason for this phenomenon may be the directional dependency of strain conditioning. Preliminary observations suggest that strain conditioning has more effect in the fiber direction (that is generally the stiffer direction) and makes the tissue to become almost isotropic.

## CONCLUSIONS

The mechanical behavior of brain tissue in shear was shown to be nonlinearly viscoelastic. Two third-order nonlinear models were developed to describe this behavior: a fully nonlinear model with product-form multiple hereditary integrals and a quasilinear viscoelastic model. The fully nonlinear model was shown to be superior especially at frequencies above 44 Hz. The elastic response of the quasilinear model showed strain hardening for shear strains above 10%.

It was shown that finite strains introduce nonrecoverable changes in the material properties of brain tissue that were referred to as strain conditioning. Under strain conditioning the magnitude of the linear complex modulus decreased and its phase increased to asymptotic values. The discrepancies observed in the mechanical properties of brain tissue in the previous studies and also the threshold of its functional failure under mechanical loading were shown to be related to the strain conditioning effect.

## ACKNOWLEDGEMENTS

This work was partially supported by the American Association of Automobile Manufacturers.

## REFERENCES

- ARBOGAST, K. B., and MARGULIES, S. S., (1998). Material Characterization of Brainstem from Oscillatory Shear Tests. *J. Biomechanics*, **31**, 801-807.
- DARVISH, K. K., (2000). Characterization of Nonlinear Viscoelastic Properties of Brain Tissue Using Forced Vibrations. Ph.D. Dissertation, University of Virginia, Charlottesville, VA.
- DONNELLY, B., and MEDIGE, J., (1997). Shear Properties of Human Brain Tissue. *J. Biomech. Eng.*, **119**, 423-432.
- FALLENSTEIN, G. T., HULCE, V. D., and MELVIN, J. W., (1969). Dynamic Mechanical Properties of Human Brain Tissue. *J. Biomechanics*, **2**, 217-226.
- FINDLEY, W. N., LAI, J. S., and ONARAN, K., (1976). *Creep and Relaxation of Nonlinear Viscoelastic Materials*. North-Holland Publishing Company.
- FUNG, Y. C., (1993). *Biomechanics: Mechanical Properties of Living Tissues*. Springer-Verlag.
- GALFORD, J. E., and MCELHANEY, J. H., (1969). Some Viscoelastic Properties of Scalp, Brain, and Dura. ASME paper No. 69-BHF-7.
- GENNARELLI, T. A., (1993). Mechanism of Brain Injury. *The Journal of Emergency Medicine*, **11**, 5-11.
- LOCKETT, F. J., (1972). *Nonlinear Viscoelastic Solids*. Academic Press.
- MARGULIES, S. S., (1987). Biomechanics of Traumatic Coma in the Primate. Ph.D. Dissertation in Bioengineering, University of Pennsylvania.
- MEANEY, D. F., SMITH, D. H., SHREIBER, D. I., BAIN, A. C., MILLER, R. T., ROSS, D. T., and GENNARELLI, T. A., (1996). Biomechanical Analysis of Experimental Diffuse Axonal Injury. *Traumatic Brain Injury: Bioscience and Mechanics*, F. A. Bandak *et al.* (eds.). Mary Ann Liebert Inc., Larchmont, NY, 167-172.
- MENDIS, K. K., STALNAKER, R. L., and ADVANI, S. H., (1995). A Constitutive Relationship for Large Deformation Finite Element Modeling of Brain Tissue. *J. Biomech. Eng.*, **117**, 279-285.
- NAKADA, O., (1960). Theory of Nonlinear Responses. *J. Physical Society of Japan*, **15**, 2280.
- NATIONAL INSTRUMENTS, (1998). *LabVIEW Function and VI Reference Manual*. ver. 5.1.
- PRANGE M. T., MEANY, D. F., and MARGUILES, S. S., (1998). Directional Properties of Gray and White Brain Tissue Undergoing Large Deformation. *Advances in Bioengineering*, ASME, BED- **39**, 151-152.

- SHUCK, L. Z., and ADVANI, S. H., (1972). Rheological Response of Human Brain Tissue in Shear. *ASME Journal of Basic Engineering*, **94**, 905-911.
- SPENCE, D. A., (1973). Nonlinear Wave Propagation in Viscoelastic Materials. *Nonlinear Elasticity*, Dickey, R. W. (ed.). Academic Press.
- STALNAKER, R. L., (1969). Mechanical Properties of the Head. Ph.D. Dissertation, West Virginia University, Morgantown, W. Va..
- TAKHOUNTS, E. G., (1998). The Experimental Determination of Constitutive Equations of Human and Bovine Brain Tissue. Ph.D. Dissertation, University of Virginia, Charlottesville, VA.
- THIBAUT, L. E., GENNARELLI, T. A., MARGULIES, S., MARCUS, J., and EPPINGER, R., (1990). The strain dependent pathological consequences of inertial loading on central nervous system tissue. *Proceedings of the 1990 International IRCOBI conference on the Biomechanics of Impacts*.
- UENO, K., MELVIN, J. W., LI, L., and LIGHTHALL, J. W., (1996). Development of Tissue Level Brain Injury Criteria by Finite Element Analysis. *Traumatic Brain Injury: Bioscience and Mechanics*. F. A. Bandak *et al.*, (eds.). Mary Ann Liebert Inc., Larchmont, NY, 155-166.
- WANG, C. H., and WINEMAN, A. S., (1972). A Mathematical Model for the Determination of Viscoelastic Behavior of Brain *in vivo*-1 Oscillatory Response. *J. Biomechanics*, **5**, 431-446.

**APPENDIX**

The values of the three frequency components associated with the frequency combination indices that were used for determination of the third-order complex moduli of samples 2, 3, and 6 are given in Table A-1.

Table A-1. Frequency Combination Indices (FCI).

Frequencies (Hz)	$f_i$	$f_n$	$f_m$	FCI	Frequencies (Hz)	$f_i$	$f_n$	$f_m$	FCI	Frequencies (Hz)	$f_i$	$f_n$	$f_m$	FCI
1	1	1	1	1	27,12,1	27	12	1	36	47	47	47	71	
5,1	5	5	1	2		27	-	1	37	63,12	63	63	12	72
	5	5	-1	3		27	12	-1	38		63	63	-	73
	5	1	1	4		27	-	-1	39		63	12	12	74
	5	-1	-1	5	27,12,5	27	12	5	40		63	-	-	75
5	5	5	5	6		27	-	5	41	63,27	63	63	27	76
12,1	12	12	1	7		27	12	-5	42		63	63	-	77
	12	12	-1	8		27	-	-5	43		63	27	27	78
	12	1	1	9	27	27	27	27	44		63	-	-	79
	12	-1	-1	10	39,5	39	39	5	45	63,27,12	63	27	12	80
12,5	12	12	5	11		39	39	-5	46		63	-	12	81
	12	12	-5	12		39	5	5	47		63	27	-	82
	12	5	5	13		39	-5	-5	48		63	-	-	83
	12	-5	-5	14	39,12	39	39	12	49	63	63	63	63	84
12,5,1	12	5	1	15		39	39	-	50	73	73	73	73	85
	12	-5	1	16		39	12	12	51	87,12	87	87	12	86
	12	5	-1	17		39	-	-	52		87	87	-	87
	12	-5	-1	18	39,12,5	39	12	5	53		87	12	12	88
12	12	12	12	19		39	-	5	54		87	-	-	89
	12	-5	-1	18		39	12	-5	55	87,27	87	87	27	90
27,1	27	27	-1	21		39	-	-5	56		87	87	-	91
	27	1	1	22	39,27	39	39	27	57		87	27	27	92
	27	-1	-1	23		39	39	-	58		87	-	-	93
	27	5	5	24		39	27	27	59	87,27,12	87	27	12	94
	27	27	-5	25		39	-	-	60		87	-	12	95
	27	5	5	26	39,27,5	39	27	5	61		87	27	-	96
	27	-5	-5	27		39	-	5	62		87	-	-	97
	27	5	1	28		39	27	-5	63	87	87	87	87	98
27,5,1	27	-5	1	29		39	-	-5	64	98	98	98	98	99
	27	5	-1	30	39,27,12	39	27	12	65	99	99	99	99	100
	27	-5	-1	31		39	-	12	66					
27,12	27	27	12	32		39	27	-	67					
	27	27	-	33		39	-	-	68					
	27	12	12	34		39	39	39	69					
	27	-	-	35	44	44	44	44	70					

